Predicting the Efficacy of Stalk Cells Following Leading Cells Through a Micro-Channel Using Morphoelasticity and a Cell Shape Evolution Model

PENG, Qiyao; VERMOLEN, Fred & Weihs, D. (2023) Predicting the Efficacy of Stalk Cells Following Leading Cells Through a Micro-Channel Using Morphoelasticity and a Cell Shape Evolution Model. In: COMPUTER METHODS, IMAGING AND VISUALIZATION IN BIOMECHANICS AND BIOMEDICAL ENGINEERING II, SPRINGER INTERNATIONAL PUBLISHING AG, p. 112 -122.

DOI: 10.1007/978-3-031-10015-4_10
Handle: http://hdl.handle.net/1942/38931

Predicting the Efficacy of Stalk Cells Following Leading Cells through a Micro-Channel Using Morphoelasticity and a Cell Shape Evolution Model

Q. Peng[1,2,3] and F. J. Vermolen[3,2] D. Weihs[4]

[1] Mathematical Institute, Leiden University, Niels Bohrweg 1, 2333 CA, The Netherlands. q.peng@math.leidenuniv.nl
[2] Delft Institute of Applied Mathematics, Delft University of Technology, Mekelweg 4, 2628 CD, Delft, The Netherlands
[3] Computational Mathematics Group, Department of Mathematics and Statistics, Faculty of Science, Hasselt University, Campus Diepenbeek, Agoralaan Gebouw D, 3590 BE Diepenbeek, Belgium. fred.vermolen@uhasselt.be
[4] Faculty of Biomedical Engineering, Technion-Israel Institute of Technology, 3200003 Haifa, Israel. daphnew@technion.ac.il

Abstract. Cancer cell migration between different body parts is the driving force behind cancer metastasis, which causes mortality of patients. Migration of cancer cells often proceeds by penetration through narrow cavities in possibly stiff tissues. In our previous work [12], a model for the evolution of cell geometry is developed, and in the current study we use this model to investigate whether followers among (cancer) cells benefit from leading (cancer) cells during transmigration through micro-channels and cavities. Using Wilcoxon's signed-rank text on the data collected from Monte Carlo simulations, we conclude that the transmigration time for the stalk cell is significantly smaller than for the leading cell with a p-value less than 0.0001, for the modelling set-up that we have used in this study.

Keywords: Cell metastasis, Evolution of cell geometry, Morphoelasticity, Agent-based model

1 Introduction

Cells are complex viscoelastic objects, of which the shape is maintained by its boundaries. Generally speaking, the cell shape is an outcome of a local balance between reaction and protrusion [3]. Therefore, cells can deform as a result of external stimuli, for instance, cell-substrate adhesion, biochemical signaling and forces exerted on the cell surface [9, 10].

When cells migrate, in particular, when a cancer cell invades and migrates through a narrow and stiff cavity, it has to deform to adapt to the obstacles. More invasive cancer cells appear to be more pliable and dynamic both internally

[4] and externally [5, 2, 15, 10], hence, they are able to adjust their cytoskeleton and geometry significantly, which could lead to possible diagnosis for cancer. Furthermore, it has been observed that cancer cells exert a significantly larger traction forces on their direct environment than benign cells do [8].

In our previous work [12], we developed a phenomenological formalism to model the evolution of the cell geometry, where we included the morphoelasticity model to describe the possibly permanent impact of cellular forces on the extracellular matrix. In this manuscript, we consider cells migrating through a microtube and the objective is to reproduce the experiments by Mak et al. [7]. In our computational setting and in the experiments [7], the width of the micro-channel is smaller than the cell size. Therefore, Hertz' contact model in combination with friction is used in order to account for the mechanical contact between channel wall and cell membrane (cell boundary).

In this study, the model by Peng et al. [12] is used and applied to a deformable channel that is subject to plastic deformation. The idea is that the first cells make the channel permanently wider, which is modelled by the use of morphoelasticity, so that cells that arrive later can transmigrate through the channel more easily and hence faster. The objective of this study is to quantify the decrease of transmigration of later cells with respect to the transmigration time of the early cells.

The manuscript is structured as follows: Section 2 summarizes the model developed in [12] regarding the evolution of the cell geometry. In Section 3, we present an application of the model where two cells consecutively penetrate through a flexible channel as well as the results from Monte Carlo simulations regarding the penetration time of the first and second cells through the channel. Afterwards, some conclusions are drawn in Section 4.

2 Mathematical Models

We present a brief summary of the model that has been developed in our previous work. For more details about the model, we refer to Peng et al. [12].

2.1 Cell Cytoskeleton

First we only consider the contribution from the cell stiffness to the movement of nodal points on the cell membrane. We assume that the cell maintains its geometry by a series of elastic springs that connect the cell centre and the nodal points on the cell boundary; see Figure 1 for an illustration. Together with the rotation matrix, the displacement of the nodal point j on the cell boundary is given by

$$d\boldsymbol{x}_j = E_c(\boldsymbol{x}_c(t) + \boldsymbol{B}(\tilde{\phi})\hat{\boldsymbol{x}}_j - \boldsymbol{x}_j(t))dt. \tag{1}$$

Here, E_c is the stiffness of the spring that connects the nodal point and cell centre, $\hat{\boldsymbol{x}} = \boldsymbol{x}_c(t) - \tilde{\boldsymbol{x}}_j(t)$ is the vector connecting the equilibrium position of nodal point i on the cell membrane to the cell centre, $\boldsymbol{x}_c$ is the central position

of the cell and $\tilde{\boldsymbol{x}}_j$ represents the equilibrium position of the nodal point j corresponding to the cell centre $\boldsymbol{x}_c$, and $\boldsymbol{B}(\tilde{\phi})$ describes the rotation of the cell, where $\boldsymbol{B}(\phi)$ is defined by

$$\boldsymbol{B}(\phi) = \begin{pmatrix} \cos(\phi) & -\sin(\phi) \\ \sin(\phi) & \cos(\phi) \end{pmatrix}, \tag{2}$$

such that ϕ can be computed from

$$\tilde{\phi} = \arg \min_{\phi \in [0,2\pi)} \left(\sum_{i=1}^{N} \| B(\phi)\tilde{\boldsymbol{x}}_i(t) - \boldsymbol{x}_i(t) \|^2 \right). \tag{3}$$

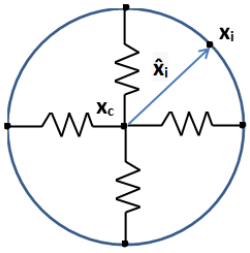

Fig. 1: A schematic of the cell cytoskeleton, which is kept by a series of springs.

2.2 Chemotaxis and Random Walk

There are various cues invoking cell migration, and one of them is chemotaxis, which provides the cell with a tendency to migrate towards (positive chemotaxis) or away from (negative chemotaxis) the gradient of a chemical. Just like in Peng et al. [12], we use a point source that secretes a chemical at the end of the micro-channel. The concentration of the chemical is modelled by a reaction-diffusion equation with a point source in open domain Ω with boundary $\partial\Omega$:

$$\begin{cases} \dfrac{\partial c(\boldsymbol{x},t)}{\partial t} + \nabla \cdot (\boldsymbol{v}c(\boldsymbol{x},t)) - \nabla \cdot (D\nabla c(\boldsymbol{x},t)) = k\delta(\boldsymbol{x}(t) - \boldsymbol{x}_s), \text{ in } \Omega,\ t > 0, \\ c(\boldsymbol{x},0) = 0, \text{in } \Omega,\ t = 0, \\ \dfrac{\partial c}{\partial \boldsymbol{n}} + \kappa_s c = 0, \text{on } \partial\Omega, t > 0, \end{cases} \tag{4}$$

where $c(\boldsymbol{x},t)$ is the concentration of the signalling molecule; D is the diffusion rate which has been taken constant in the current study; k is the secretion rate

of the signal source; $\boldsymbol{x}_s$ is the position of the source; $\delta(\boldsymbol{x}(t))$ is the Dirac Delta distribution, which is defined by

$$\delta(\boldsymbol{x}) = 0, \text{ for } \boldsymbol{x} \neq \boldsymbol{0},$$

and constrained to satisfy the identity that

$$\int_{\Omega} \delta(\boldsymbol{x}) d\Omega = 1, \text{ if } \boldsymbol{0} \in \Omega,$$

for any dimensionality (note that Ω is open); $\boldsymbol{v}$ is the displacement velocity of the substrate that results from the cellular forces exerted on their surroundings. The velocity is computed by solving the balance of the momentum, which will be discussed in the Section 2.3.

Together with the random displacement of the cell, which is described by a vector-Wiener process and the contribution from the cell stiffness, the displacement of a nodal point on the cell membrane is modelled by

$$d\boldsymbol{x}_j = E_c(\boldsymbol{x}_c(t) + \boldsymbol{B}(\tilde{\phi})\hat{\boldsymbol{x}}_j - \boldsymbol{x}_j(t))dt + \beta \frac{\nabla c(\boldsymbol{x}_j)}{\|\nabla c(\boldsymbol{x}_j)\| + \gamma} dt + \sigma_{rw} d\boldsymbol{W}(t), \quad (5)$$

where β is the chemotaxis sensitivity parameter, γ is a small positive constant to prevent division by zero, and σ_{rw} is the random walk parameter (in particular, the standard deviation of the random fluctuation, of which the square is proportional to the cell diffusion constant).

2.3 Force Balance and Friction

It has been documented in many studies, see for instance [8], that cancer cells exert forces on the immediate environment and that they are able to change biochemical properties of their immediate environment. We incorporate the forces that are exerted by the (migrating) cells on the walls of the micro-channel. We accommodate for the plastic nature of the resulting deformations by the use of a morphoelastic formalism. The morphoelastic model combines a mechanical balance, where viscoelasticity has been included, with an evolutionary equation for the effective Eulerian strain. This results into the following set of partial differential equations:

$$\begin{cases} \rho[\dfrac{D\boldsymbol{v}}{Dt} + \boldsymbol{v}(\nabla \cdot \boldsymbol{v})] - \nabla \cdot \boldsymbol{\sigma} = \boldsymbol{f}_m, \text{in } \Omega,\ t > 0, \\ \dfrac{D\boldsymbol{\varepsilon}}{Dt} + \boldsymbol{\varepsilon}\,\mathrm{skw}(\boldsymbol{L}) - \mathrm{skw}(\boldsymbol{L})\boldsymbol{\varepsilon} + [\mathrm{tr}(\boldsymbol{\varepsilon}) - 1]\,\mathrm{sym}(\boldsymbol{L}) = -\alpha\boldsymbol{\varepsilon}, \text{in } \Omega,\ t > 0, \\ \boldsymbol{v}(\boldsymbol{x}, t) = \boldsymbol{0}, \text{on } \partial\Omega,\ t > 0, \\ \boldsymbol{v}(\boldsymbol{x}, 0) = \boldsymbol{0}, \text{in } \Omega,\ t = 0, \\ \boldsymbol{\varepsilon}(\boldsymbol{x}, 0) = \boldsymbol{0}, \text{in } \Omega,\ t = 0, \end{cases} \quad (6)$$

where ρ is the density of the extracellular matrix, $\boldsymbol{L} = \nabla \boldsymbol{v}$ and α is a non-negative constant, and $\boldsymbol{\varepsilon}$ is the effective Eulerian strain tensor that is to be

solved. Note that if $\alpha = 0$, then as soon as the force $\boldsymbol{f}_m = \boldsymbol{0}$, then the tissue will gradually recover to its original shape and volume. Here, $\frac{Dy}{Dt} = \frac{\partial y}{\partial t} + \boldsymbol{v} \cdot \nabla y$ is material derivative where y is any scalar field and $\boldsymbol{v}$ is the migration velocity of any point within the domain of computation. In order to have a fixed boundary, we use a homogeneous Dirichlet boundary condition for the velocity. From a mechanical point of view, we treat the computational domain as a continuous linear isotropic domain. Further, as a result of the presence of liquid phases in the tissue, the mechanical balance is also subject to viscous, that is friction, effects. Therefore, we use Kelvin–Voigt's viscoelastic dashpot model, of which the stress tensor reads as

$$\begin{aligned} \boldsymbol{\sigma} &= \boldsymbol{\sigma}_{elas} + \boldsymbol{\sigma}_{visco} \\ &= \frac{E}{1+\nu_s}\{\boldsymbol{\varepsilon} + \operatorname{tr}(\boldsymbol{\varepsilon})[\frac{\nu_s}{1-2\nu_s}]\boldsymbol{I}\} + \mu_1 \operatorname{sym}(\boldsymbol{L}) + \mu_2 \operatorname{tr}(\operatorname{sym}(\boldsymbol{L}))\boldsymbol{I}, \end{aligned} \tag{7}$$

where ν_s is the Possion's ratio of the substrate, $\boldsymbol{\varepsilon}$ is the effective Eulerian strain tensor, μ_1 and μ_2 are the shear and bulk viscosities respectively. The morphoelasticity model solves two (nonlinear) partial differential equations and both velocity $\boldsymbol{v}$ and strain tensor $\boldsymbol{\varepsilon}$ are unknowns. The displacement of the domain can be approximated by numerically integrating the velocity over time: $\boldsymbol{u}(t) = \int_0^t \boldsymbol{v}(s)ds$.

We consider cells transmigrating through a deformable channel. The cell boundaries exert forces on the channel wall and the channel wall exerts reaction forces on the cell boundaries. As mentioned earlier, the cell boundary points are connected to the cell centre by springs and further these points are connected to their immediate neighboring points on the cell boundary. Similar to Peng et al. [12], we assume that $N_l = \{i_1, \ldots, i_m\}$ and $N_p = \{j_1, \ldots, j_{m+1}\}$, respectively, are the line segments and nodal points of the cell membrane that are in mechanical contact with the wall of the channel. Then the force $\boldsymbol{f}_m$ in Eq (6) reads as

$$\boldsymbol{f}_m(\boldsymbol{x}, t) = \sum_{i \in N_l} Q\boldsymbol{n}(\boldsymbol{x}^i(t))\delta(\boldsymbol{x}(t) - \boldsymbol{x}^i(t))\Delta\Gamma^i, \tag{8}$$

where Q is the magnitude of the traction force per unit length that is exerted by the cell, $\boldsymbol{n}(\boldsymbol{x}(t))$ is the unit outward pointing vector at point $\boldsymbol{x}(t)$, $\boldsymbol{x}^i(t)$ is the midpoint of line segment i, $\delta(\boldsymbol{x}(t))$ is the Dirac delta distribution and $\Delta\Gamma^i$ is the length of line segment i.

Besides the pushing traction forces that the cell exerts on the channel, the wall exerts a friction and compressive force on the boundary of the cell. This friction force is assumed to be proportional to the forcing between the walls of the cell and the channel and hence both the spring force contribution of the cell and the force exerted on the channel wall are incorporated. Therefore, the friction $\boldsymbol{f}_f(\boldsymbol{x}, t)$, which is only at the nodal point $j \in N_p = \{j_1, \ldots, j_{m+1}\}$, is expressed as a sum of two aforementioned forces:

$$\boldsymbol{f}_f(\boldsymbol{x}_j, t) = \boldsymbol{f}_m(\boldsymbol{x}_j, t) + E_c(\boldsymbol{B}(\tilde{\phi})\hat{\boldsymbol{x}}_j - \boldsymbol{x}_j(t)). \tag{9}$$

Therefore, combining with the passive convection of the substrate and the effect of the friction, Eq (1) is now given by

$$\begin{aligned} d\boldsymbol{x}_j = E_c(\boldsymbol{x}_c(t) + \boldsymbol{B}(\tilde{\phi})\hat{\boldsymbol{x}}_j - \boldsymbol{x}_j(t))dt + \beta \frac{\nabla c(\boldsymbol{x}_j)}{\|\nabla c(\boldsymbol{x}_j)\| + \gamma} dt + \boldsymbol{v}(\boldsymbol{x}_j(t))dt \\ - \mu_f \|\boldsymbol{f}_f(\boldsymbol{x}_j(t))\| \cdot (d\boldsymbol{x}_j(t), \boldsymbol{\tau}_{ob}(\boldsymbol{x}_j(t)))\boldsymbol{\tau}_{ob}(\boldsymbol{x}_j(t)) + \sigma_{rw} d\boldsymbol{W}(t), \end{aligned} \tag{10}$$

where μ_f is the friction coefficient, and $\boldsymbol{\tau}_{ob}(\boldsymbol{x})$ is the unit tangential vector of the obstacle boundary. We bear in mind that that the forces are only exerted on the direct environment of the cell if both end points of the line segment are in direct contact with the channel wall; similarly, friction is only incorporated on a nodal point that is in direct contact with the channel wall.

3 Applications and Numerical Results

In our previous work [12], we presented several applications of the model, for instance, cell migration, cell differentiation and cell penetrating through a microtube. In this manuscript, we consider a flexible channel, which deforms due to the traction forces that a cell exerts on the channel wall. Figure 2(a) shows the initial settings of the simulation, where the cell is initially located in one side of the channel and migrates towards the gradient of the concentration of the signalling molecules through the channel. Once the first cell exits the channel, it will be discarded in further computations, and the second cell will start migrating from its initial position, i.e. the position where the red circle is, in Figure 2(a). The parameter values are shown in Table 1. The horizontal channel is determined by

$$y = \pm(3.5 + \sin(0.5x))\mu m, \ x \in (-60, 60)\mu m.$$

Several screenshots are shown in Figure 2, which shows the locations of the cells and the shape of the cell and the channel. In Figure 2(b), the part of the channel that the first cell has penetrated, has clearly expanded. Once the first cell has entirely left the channel, it is disregarded in further calculations, and simultaneously the second cell appears at the initial position (the red circle), see Figure 2(d) and 2(e). The plastic deformation that has been caused by the first cell makes the second cell transmigrate through the micro-channel more easily because less force needs to be applied by the cell. From Figure 2, it is observed that the channel is slightly deformed in the direction of the migration of the cells.

Due to the significant deformation of the channel, we are interested in whether the second cell can benefit from the first cell expanding the flexible channel, that is, whether it takes less time for the second cell to penetrate through the channel than for the first cell, see Figure 2(e) – (h). We carry out Monte Carlo simulations without taking any other input parameters as random variables. Hence, the only stochastic process in the model is the random walk contribution to migration of

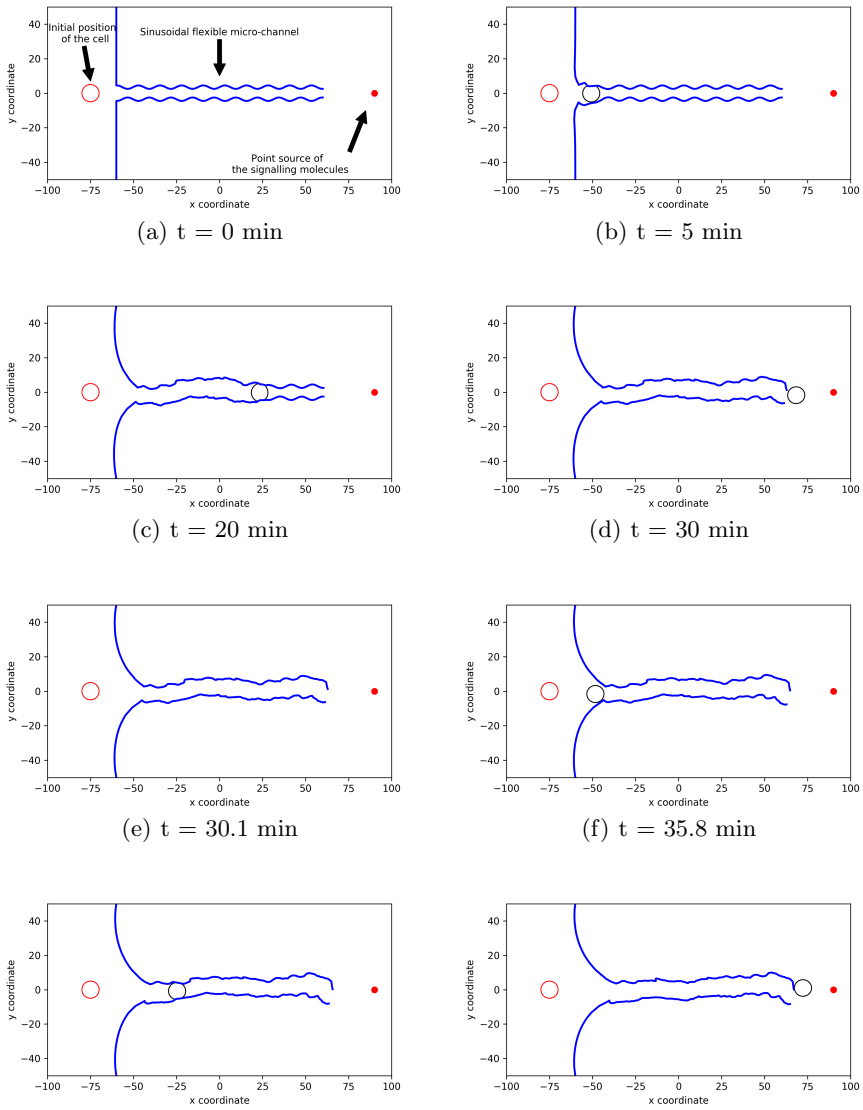

(a) t = 0 min (b) t = 5 min

(c) t = 20 min (d) t = 30 min

(e) t = 30.1 min (f) t = 35.8 min

(g) t = 40.8 min (h) t = 61.9 min

Fig. 2: Screenshots of the simulation at different moments when two cells penetrate the flexible channel sequentially. The red dot at the very right position with coordinates $(90, 0)$ ***in the figure is the point source of the signalling molecules; blue curves are the deformed channel, which is initially sinusoidal; red circle represents the initial position and shape of the cells.***

Table 1: Parameter values used in the computational simulations

Parameter	Description	Value	Units	Source
P_0	Maximal traction force exerted by cells	10.4	$kg \cdot \mu m/h^2$	[6]
μ_f	Cell friction coefficient	0.03	–	[1]
ν_s	Poisson's ratio of the substrate	0.49	–	[6]
k	Secretion rate of the cell-attractive signal	2.5	$kg/(\mu m^3 \cdot min)$	[11]
κ_s	Parameter in Robin's boundary condition to solve Eq (4)	100	μm^{-1}	[11]
μ_1	Shear viscosity of the ECM	33.783	–	[11]
μ_2	Bulk viscosity of the ECM	22.523	–	[11]
Estimated parameter values				
$x0$	Length of the computational domain in x-axis	200	μm	
$y0$	Length of the computational domain in x-axis	100	μm	
Δt	Time step	0.1	min	
E_s	Substrate elasticity	50	$kg/(\mu m \cdot min^2)$	
E_c	Cell elasticity and the stiffness of the springs in the cell cytoskeleton	10	$kg/(\mu m \cdot min^2)$	
R	Cell radius	5	μm	
β	Maximal mobility of points on cell membrane	5	min^{-1}	
D	Diffusion rate of the signal	233.2	$\mu m^2/min$	
N	Number of nodal points on the cell membrane	40	–	
σ_{rw}	Weight of random walk	1	–	
α	Degree of permanent ECM deformation in Eq (6)	2	–	

the cell. We collected 1130 samples regarding the penetration time of each cell through the channel. The box plot and density plot of the data are presented in Figure 3, respectively. From these plots, it is hard to conclude whether the second cell takes significantly less time than the first cell to migrate through the channel. This seemingly small difference between the transmigration times of the second and first cells is probably the result of the thickness of the channel being comparable to the cell diameter. We expect that the differences in transmigration times increase if the channel width is much smaller than the cell size. Of course, this trend will depend on the amount of plasticity in the deformation of the channel. This will be a topic for further research. Furthermore, according to Shapiro's test [14], neither of the dataset is normally distributed with p-value less than 0.05. Therefore, instead of the t-test, we use Wilcoxon's signed-rank

test for these two paired samples, since Wilcoxon's signed-rank test [13] does not require normality of the data.

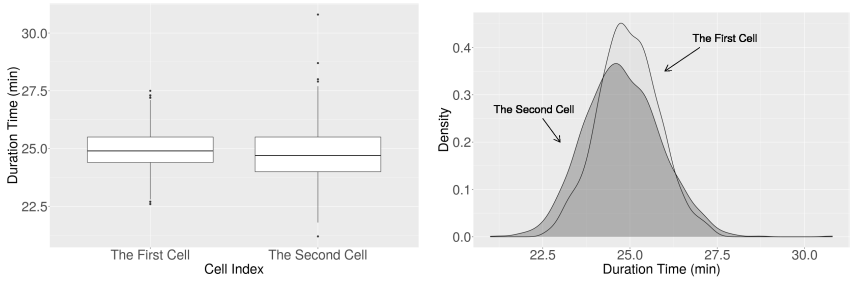

(a) Box Plot (b) Density Plot

Fig. 3: Empirical plots of the data collected from the Monte Carlo simulations. (a) Box plot shows the median (middle line), 25% ***(*** Q_1 ***) and*** 75% ***(*** Q_3 ***) percentile (lower and upper bound of the box), the minimum (*** $Q_1 - 1.5\dfrac{Q_3 - Q_1}{2}$ ***) and maximum (*** $Q_3 + 1.5\dfrac{Q_3 - Q_1}{2}$ ***) of the data excluding the outliers (verticle lines) and outliers (dots). (b) Estimated probability density of the penetration time for the first and the second cell, respectively.***

Table 2 displays the statistical results from the Wilcoxon's signed-rank test of the two paired dataset regarding the penetration time in the channel. The p-value is much smaller than the significance level 0.05, therefore, based on the data collected from the Monte Carlo simulation, we conclude that the second cell does benefit from the first cell expanding the channel.

Null Hypothesis $(H_0 : T_1 = T_2)$	There is no difference in penetration time for both cells.
Alternative Hypothesis $(H_1 : T_1 > T_2)$	The second cell has shorter penetration time than the first cell.
$p - value = \mathbb{P}(Data \mid H_0) = 1.158 \times 10^{-5}$	

Table 2: Statistical results of Wilcoxon's signed-rank test on the paired dataset of penetration time of each cell. T_1 ***and*** T_2 ***represent the penetration time of the first and second cell, respectively.***

4 Discussion and Conclusions

Our previously developed model for the evolution of cell geometry has been used to investigate whether followers among (cancer) cells benefit from leading (cancer) cells during transmigration through micro-channels and cavities. Since cell migration is subject to randomness, Monte Carlo simulations have been done to estimate the probability density of penetration times for both the leading and stalk cells. Using Wilcoxon's signed-rank test, it has been concluded that the transmigration time for the stalk cell is significantly smaller than for the leading cell with a p-value of less than 0.0001. The physical explanation is that the first (leading) cell deforms the micro-channel plastically so that the channel is wider when the second (stalk) cell transmigrates through the channel. The second cell has the advantage that it needs to exert fewer forces than the first cell. This effect could possibly even be amplified if metabolism would be taken into account.

We realize that we have shown the (Monte Carlo) results for one modelling set-up only. All input variables have been fixed and all differences in simulation runs were exclusively caused by the random nature of cell migration through the Wiener process (white noise – random walk). Nevertheless, we may conclude via Wilcoxon's signed-rank test that the current simple 'toy model' predicts a significant difference between the transmigration times of the second and first cell, from which it is concluded that the second cell transmigrates more easily than the first cell for the current modelling set-up. In our future Monte Carlo simulations, we will add uncertainties in the channel width, channel length, Young's modulus of the ECM, distance between the initial cell positions and the channel, distance between the consecutive cells, amount of plasticity in the deformation and possibly more (biophysical) parameters by the use of prior statistical distributions.

Bibliography

[1] T. E. Angelini, A. C. Dunn, J. M. Urueña, D. J. Dickrell, D. L. Burris, and W. G. Sawyer. Cell friction. Faraday Discussions, 156:31, 2012. doi: 10.1039/c2fd00130f. URL https://doi.org/10.1039/c2fd00130f.

[2] S. E. Cross, Y.-S. Jin, J. Rao, and J. K. Gimzewski. Nanomechanical analysis of cells from cancer patients. Nature Nanotechnology, 2(12):780–783, Dec. 2007. doi: 10.1038/nnano.2007.388. URL https://doi.org/10.1038/nnano.2007.388.

[3] H. Ebata, A. Yamamoto, Y. Tsuji, S. Sasaki, K. Moriyama, T. Kuboki, and S. Kidoaki. Persistent random deformation model of cells crawling on a gel surface. Scientific Reports, 8(1), Mar. 2018. doi: 10.1038/s41598-018-23540-x. URL https://doi.org/10.1038/s41598-018-23540-x.

[4] N. Gal and D. Weihs. Intracellular mechanics and activity of breast cancer cells correlate with metastatic potential. Cell Biochemistry and Biophysics, 63(3):199–209, May 2012. doi: 10.1007/s12013-012-9356-z. URL https://doi.org/10.1007/s12013-012-9356-z.

[5] J. Guck, S. Schinkinger, B. Lincoln, F. Wottawah, S. Ebert, M. Romeyke, D. Lenz, H. M. Erickson, R. Ananthakrishnan, D. Mitchell, J. Käs, S. Ulvick, and C. Bilby. Optical deformability as an inherent cell marker for testing malignant transformation and metastatic competence. Biophysical Journal, 88(5):3689–3698, May 2005. doi: 10.1529/biophysj.104.045476. URL https://doi.org/10.1529/biophysj.104.045476.

[6] D. Koppenol. Biomedical implications from mathematical models for the simulation of dermal wound healing. PhD-thesis at the Delft University of Technology, the Netherlands, 2017.

[7] M. Mak, C. A. Reinhart-King, and D. Erickson. Elucidating mechanical transition effects of invading cancer cells with a subnucleus-scaled microfluidic serial dimensional modulation device. Lab Chip, 13(3):340–348, 2013. doi: 10.1039/c2lc41117b. URL https://doi.org/10.1039/c2lc41117b.

[8] S. Massalha and D. Weihs. Metastatic breast cancer cells adhere strongly on varying stiffness substrates, initially without adjusting their morphology. Biomechanics and Modeling in Mechanobiology, 16(3):961–970, Dec. 2016. doi: 10.1007/s10237-016-0864-4. URL https://doi.org/10.1007/s10237-016-0864-4.

[9] A. Mogilner and K. Keren. The shape of motile cells. Current Biology, 19 (17):R762–R771, Sept. 2009. doi: 10.1016/j.cub.2009.06.053. URL https://doi.org/10.1016/j.cub.2009.06.053.

[10] E. Paluch and C.-P. Heisenberg. Biology and physics of cell shape changes in development. Current Biology, 19(17):R790–R799, Sept. 2009. doi: 10.1016/j.cub.2009.07.029. URL https://doi.org/10.1016/j.cub.2009.07.029.

[11] Q. Peng and F. Vermolen. Agent-based modelling and parameter sensitivity analysis with a finite-element method for skin contraction. Biomechanics and Modeling in Mechanobiology, pages 1–27, 2020.

[12] Q. Peng, F. J. Vermolen, and D. Weihs. A formalism for modelling traction forces and cell shape evolution during cell migration in various biomedical processes. Biomechanics and Modeling in Mechanobiology, Apr. 2021. doi: 10.1007/s10237-021-01456-2. URL https://doi.org/10.1007/s10237-021-01456-2.

[13] D. Rey and M. Neuhäuser. Wilcoxon-signed-rank test. In International Encyclopedia of Statistical Science, pages 1658–1659. Springer Berlin Heidelberg, 2011. doi: 10.1007/978-3-642-04898-2_616. URL https://doi.org/10.1007/978-3-642-04898-2_616.

[14] S. S. Shapiro and M. B. Wilk. An analysis of variance test for normality (complete samples). Biometrika, 52(3/4):591–611, 1965.

[15] V. Swaminathan, K. Mythreye, E. T. O'Brien, A. Berchuck, G. C. Blobe, and R. Superfine. Mechanical stiffness grades metastatic potential in patient tumor cells and in cancer cell lines. Cancer Research, 71(15):5075–5080, June 2011. doi: 10.1158/0008-5472.can-11-0247. URL https://doi.org/10.1158/0008-5472.can-11-0247.